Diamond & Related Materials 105 (2020) 107798

Contents lists available at ScienceDirect

Diamond & Related Materials

journal homepage: www.elsevier.com/locate/diamond

Study of graphene layer growth on dielectric substrate in microwave plasma torch at atmospheric pressure

Ondřej Jašek*, Jozef Toman, Jana Jurmanová, Miroslav Šnírer, Vít Kudrle, Vilma Buršíková

Department of Physical Electronics, Faculty of Science, Masaryk University, Kotlářská 2, 611 37 Brno, Czech Republic

ARTICLE INFO

Keywords:
Graphene
Microwave plasma
Ethanol
Dielectric substrate

ABSTRACT

The initial stage of graphene layer deposition on silicon oxide substrate by ethanol decomposition in dual-channel microwave plasma torch at atmospheric pressure was studied in dependence on precursor flow rate and delivered microwave power. Depending on ethanol flow rate and substrate temperature, horizontally or vertically aligned graphene nanosheets with various density could be prepared directly on dielectric substrate. In the regime with high microwave power, above 400 W, mixture of amorphous carbon particles and graphene sheets was deposited on the substrate. Prepared layers were analyzed by scanning electron microscopy (SEM), Raman spectroscopy and X-ray photoelectron spectroscopy (XPS). The microwave plasma diagnostics was carried out using optical emission spectroscopy (OES). The sample analysis showed increasing density of horizontally aligned carbon nanosheets with increasing ethanol flow rate and their delamination and transition into vertically aligned graphene sheets with increasing substrate temperature. The Raman spectroscopy analysis of layers showed presence of D (1345 cm^{-1}), G (1585 cm^{-1}) and 2D (2685 cm^{-1}) peaks with 2D/G ratio of 1.59 and full width at half maximum (FWHM) of 2D peak was 42 cm^{-1}, corresponding to few layer graphene structure. In case of amorphous nanoparticles deposition, the D* peak at 1210 cm^{-1} and D** at 1500 $sccm^{-1}$ was observed in Raman spectra with D/G ratio of 1.19 and C1s XPS spectra of carbon contained 20.4 at.% of sp^3 carbon phase in comparison to 8.3 at.% in case of graphene nanosheets layer. High D/G ratio, up to 3.5, and low intensity 2D band was characteristic for vertically aligned graphene nanosheets layers. The possibility to influence density and size of graphene nanosheets on substrate represents promising alternative for future deposition of graphene on arbitrary substrate.

1. Introduction

Graphene belongs among the most promising materials in both, fundamental and applied science [1]. Today, exfoliation from graphite crystals and chemical vapor deposition belong to most widely used methods to prepare graphene layers on the substrate [2]. These methods produce high quality layers in limited amounts or require elaborate transfer techniques to dielectric substrates. Alternative approach is controlled decomposition of organic precursors using plasma enhanced chemical vapor deposition (PECVD) [3]. Such approach enables synthesis of good quality material in reasonable amounts. It is of great interest to grow graphene layers directly on dielectric substrates. There are two main approaches to achieve growth of graphene on the dielectric substrate. First approach uses solid carbon source deposited onto a desired dielectric substrate which can be transformed into graphene films by high temperature annealing. In order to accelerate the decomposition of solid carbon sources, capping metal layers such as Cu or Ni deposited on carbon sources can be used [4]. Second approach is direct CVD of graphene on dielectric substrate with introduction of metal vapors or use of plasma enhanced CVD process. While there has been some success in these methods, the graphene nucleation density, the growth rate on dielectric substrates as compared to metallic substrates and the size of graphene single crystal domains is usually small (about few micrometers) [5]. There was also reported growth of graphene directly on dielectric substrate by PECVD where the decomposition of carbon precursor enabled growth at lower temperature, however, until now this method resulted only in limited success (450–500 °C) and small domain sizes of graphene [6,7]. Another approach to grow graphene on dielectric substrate without metallic catalyst is so called vertically aligned few layer graphene (FLG) or carbon nanowalls. Such a growth was first reported by Malesevic et al. for synthesis of FLG from mixture of methane and hydrogen in microwave PECVD [8]. Overall, wide range of plasma sources was used for synthesis of FLG including direct current (DC), radio-frequency (RF)

* Corresponding author.
E-mail address: jasek@physics.muni.cz (O. Jašek).

https://doi.org/10.1016/j.diamond.2020.107798
Received 1 November 2019; Received in revised form 3 March 2020; Accepted 3 March 2020
Available online 05 March 2020
0925-9635/

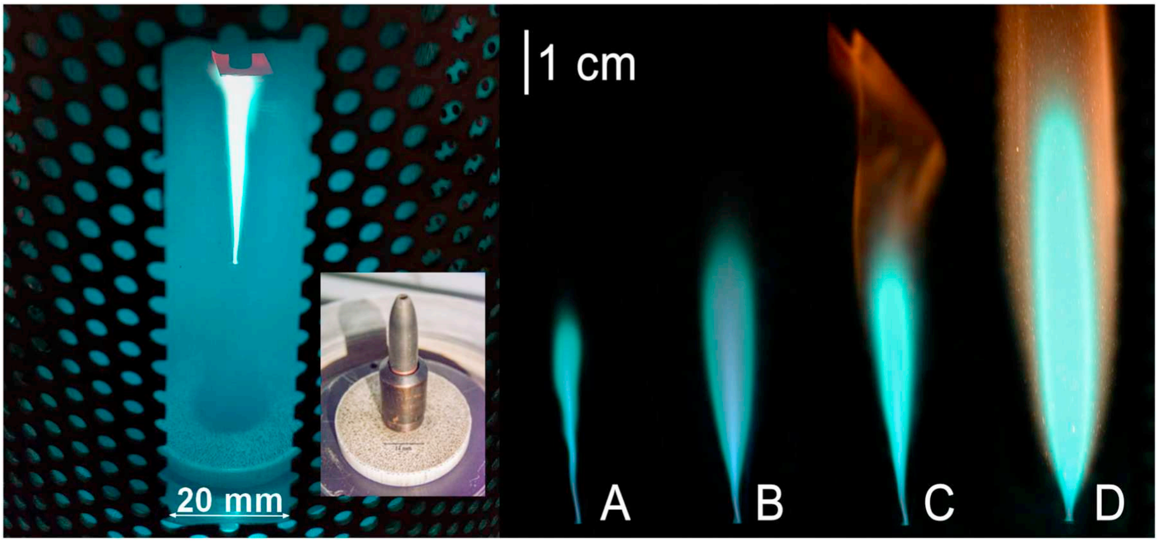

Fig. 1. Detail of carbon plasma nozzle and deposition process of graphene layer on the left and photographs of the discharge for Qc 500 sccm and a) Qs 70 sccm and P_{MW} 105 W, b) Qs 70 sccm and P_{MW} 175 W, c) Qs 140 sccm and P_{MW} 175 W and d) Qc 360 sccm, Qs 300 sccm and P_{MW} 420 W.

capacitive and inductively coupled to microwave (MW) power sources, and naturally, PECVD has become main method for FLG synthesis [9]. Typical growth pressure range is several Pascals for capacitive coupled systems to 10^3–10^4 Pa for DC and microwave powered setups. The growth temperature was limited by surface reaction kinetics and varies from 750 to 1300 K and all experiments, except MW setups, used external resistive heating for the elevation of substrate temperature. Among substrates used for deposition were silicon, quartz, metals or their combination and precursors were mixture of H_2 with hydrocarbon (CH_4, C_2H_2) or fluorocarbons, such as CF_4, CHF_3 or C_2F_6. To achieve better quality of the layer combination of oxygen containing precursors such as CO_2 and CO together with H_2 and CH_4 were used. It is worth noting that the systems used for growth of FLG are almost always low pressure systems and experiments at atmospheric pressure were only partially successful and resulted in mixture of various forms of carbon allotropes. Growth using atmospheric pressure DC normal glow discharge in Ar/CH_4 and Ar/H_2/ethanol was reported on Si, Cu and stainless steel substrate and studied by Bo et al. [10] and applied as gas sensor by Yu et al. [11]. Meško et al. [12] reported growth on Ni using atmospheric pressure DC glow PECVD in mixture of Ar/H_2/ethanol or hexane and reported growth rates as high as 100 nm per minute at 1000 K. This approach was in detail reviewed by Bo et al. [9] and recently by Vasell et al. [13] and Santhosh et al. [14]. Alternative method for the growth of graphene was developed by Dato et al. [15] concerning microwave plasma decomposition of ethanol or dimethyl ether for synthesis of graphene nanosheets in the gas phase. This method was further refined by Tatarova et al. [16] and Tsyganov et al. [17] also developed a theoretical model of the synthesis process and could simulate and experimentally map the particle and thermal fluxes in their plasma reactor. Melero et al. also showed that decomposition of ethanol in TIAGO torch at atmospheric pressure could be used for synthesis of carbon nanotubes and graphene nanosheets without use of catalyst [18,19] and efficient hydrogen generation [20]. This approach was recently extended to N-doping and the use of methane as precursor by Bundaleska et al. [21,22]. In our work we have showed that dual channel microwave plasma torch could be used for direct growth of carbon nanotubes and nanofibers on the substrate [23] and that these could be used as sensors [24] with comparable performance to graphene oxide [24,25]. In comparison with hydrocarbon precursors, the use of ethanol enables robust system for nucleation and assembly of graphene layer without the need to add another reactive gas, such as H_2, into deposition mixture. This is caused by ethanol structure of CH_3-CH_2OH, which is at high temperature, above 2000 K, decomposed predominantly into CO and H_2 molecules and C_2 species responsible for graphene nucleation and growth. This way simple, single precursor, system can be used for bottom-up synthesis of graphene with various properties. In this work we study formation of carbon based layers on dielectric substrate by decomposition of ethanol in dual-channel microwave plasma torch at atmospheric pressure. We study formation of basic building blocks directly on dielectric substrate (Si/SiO_2) in dependence on ethanol precursor flow rate, delivered microwave power and substrate temperature.

2. Materials and methods

The graphene nanosheets were synthesized by ethanol decomposition in dual-channel microwave plasma torch at atmospheric pressure. The microwave discharge was ignited inside reactor formed by quartz tube (80 mm diameter, 200 mm length) terminated by dural flanges. The discharge electrode was hollow carbon nozzle with central channel used for introduction of working gas - argon Qc (300–500 sccm) and subsequent ignition of plasma. The secondary channel (annulus with outer radius 8.4 mm and inner radius 7.7 mm) was used for introduction of carrying gas - argon Qs (35–360 sccm) with precursor (ethanol 2 to 19 mg/min) vapors into the plasma environment. Deposition time was 120 s. The layers were deposited on 10 × 10 mm one-side polished Si (100) P type, 525 mm thickness wafers from ON Semiconductor s.r.o. (Czech Republic) with 92 nm thermally oxidized SiO_2 layer and fixed in the holder during the deposition Fig. 1. More details about the experimental setup can be found in [26]. Raman spectroscopy was carried out using HORIBA LabRAM HR Evolution system with 532 nm laser, using 100× objective and 25% ND filter in the range from 1000 to 3200 cm^{-1}. Samples were imaged with TESCAN scanning electron microscope (SEM) MIRA3 with Schottky field emission electron gun equipped with secondary electron (SE) and back-scattered electron (BSE) detectors as well as Oxford Instruments EDX analyser. Transmission electron microscopy (TEM) was carried out using JEOL JEM-2100F and FEI Tecai F20 microscope. ImageJ Fiji software was used for determination of particle size and fast Fourier transform (FFT) image analysis. Particle size analysis was carried out in following sequence: image scale calibration, denoise by median filter, adaptive threshold procedure was applied for particle selection and analyze particles dialog was used for particle size determination excluding particles on image edges (area, median ferret diameter (particle size) i.e. the longest distance between any two points along the selection boundary, also known as maximum caliper). We use median value for the particle size because the particle size distribution was systematically skewed to lower values i.e. there were more smaller nanoparticles than bigger ones on the substrate. The standard deviation of the particle size distribution was large, 50% and more of the mean value, due to the broad range of size and irregular shape of the nanosheets. Atomic force microscopy (AFM) was carried out using atomic force microscope NTEGRA Prima NT-MDT in semi-contact mode. Substrate temperature was measured by K thermocouple with compensation line JUMO 901250/32-1043-1.5-300-48-2500. Optical emission spectra were recorded using a Jobin-Yvon Triax 550 spectrometer (1200 g mm^{-1}, 3600 g mm^{-1}) with an LN2 cooled CCD detector and an Avantes UL-S3648TEC-USB2 overview spectrometer with UA grating. The rotational temperature was estimated by fitting experimentally obtained CN ($B^2\Sigma^+$-$X^2\Sigma^+$) spectra at 390 nm using simulation in the Massive OES software [27]. Ethanol p.a. 99.8% from Penta was purchased from Verkon (Czech Republic). Pure gas, argon 99.998%, was purchased from Messer Technogas, s.r.o. (Czech Republic).

3. Results and discussion

3.1. Microwave plasma torch diagnostics and substrate temperature measurement

Microwave plasma at atmospheric pressure represents high temperature system reaching up to 5000 K during decomposition of ethanol as shown by Tsyganov et al. [14] and Rincon et al. [28]. At such a high temperature main products of plasma combustion of ethanol are C atoms and C_2, CO and H_2 molecules. C_2 molecules with small admixture of C_2H_x hydrocarbons are then the main precursors for the growth of carbon nanostructures. In our experiment, the concentration of these species was controlled by ethanol flow rate and absorbed microwave power delivered to the plasma (P_{MW}). The substrate temperature was above all influenced by delivered microwave power and the distance between the substrate and the discharge. It can be seen in Fig. 1 that the delivered microwave power was the main deposition parameter influencing discharge properties. The microwave power absorbed in the plasma influenced not only its shape and gas flow dynamics but also plasma temperature which increased with input power. Higher power absorption led to decomposition of carbon molecules and the ratio of C_2/C plasma species was decreasing in case of lower flow rate of ethanol precursor. On the other hand, higher flow rate of ethanol led to growth of the ratio of C_2/C even while delivered microwave power increased. The main part of the discharge was excitation zone - plasma plume, exhibiting typical green colour caused by emission of molecular C_2 Swan system between 420 and 620 nm with maximum at 517 nm. This region's length was increasing as the plasma temperature increased with absorbed microwave power.

Optical emission spectra of microwave plasma torch discharge in argon with ethanol admixture can be seen in Fig. 2. We could observe emission spectra of argon (4p-4s above 690 nm), hydrogen H_α (656.3 nm) and C atomic line at 247.8 nm. Besides main molecular bands of carbon radical C_2 Swan system ($d^3\Pi_g$-$a^3\Pi_u$) at 420–620 nm we observed molecular bands of hydroxyl radical OH ($A^2\Sigma^+$-$X^2\Pi$ 303–315 nm), second positive system of N_2 ($C^3\Pi_u$-$B^3\Pi_g$ 315–380 nm), NH ($A^3\Pi^+$-$X^3\Sigma$ 336 nm) and violet system of CN ($B^2\Sigma^+$-$X^2\Sigma^+$, 344–460 nm) as well. The presence of OH and N related species in the discharge was caused by small atmospheric impurities in the discharge chamber. The large continuum background in high power regime was caused by thermal radiation of carbon nanoparticles. The plasma temperature, i.e. neutral gas temperature, determined by fitting of rotational structure of CN ($B^2\Sigma^+$-$X^2\Sigma^+$) band at 390 nm depended linearly on delivered microwave power and saturated with increasing ethanol flow rate. The temperature increased from 3100 K for lowest Qs flow rate and lowest power (Qs 35 sccm, P_{MW} 105 W) to 4200 K for highest

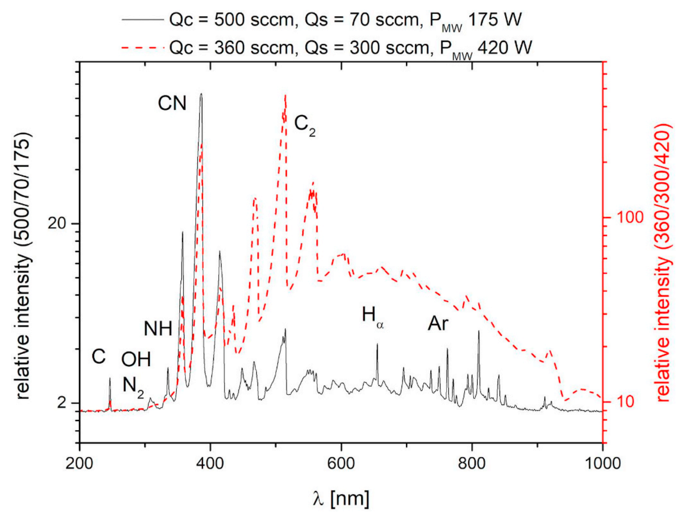

Fig. 2. Optical emission spectra of microwave plasma torch. Comparison of Qc 500 sccm, Qs 70 sccm, P_{MW} 175 W and Qc 360 sccm, Qs 300 sccm, P_{MW} 420 W.

Qs and P_{MW} values. As the plasma temperature influenced the substrate temperature, we carried out temperature measurement of the substrate placed at variable distance from the plasma discharge. Because the plasma discharge length changed, we used as a figure of merit the distance of the substrate from the plasma nozzle. It can be seen in Fig. 3, the substrate temperature was mainly influenced by plasma power i.e. proximity of the discharge itself, and only weakly depended on gas and precursor flow rates. The substrate position in the vicinity of the hot plasma zone led to sharp increase of the substrate temperature. If the substrate was placed directly into plasma hot zone it was irreversibly damaged i.e. substrate temperature increased above its melting point. In case of lower delivered microwave power, the discharge length reduced and it was possible to place the substrate to lower position but obviously, the maximum temperature of the substrate reachable without damage remained the same.

3.2. Graphene layer deposition in dependence on precursor flow

The growth of carbon layer on dielectric substrate requires formation of nucleation centers on the substrate surfaces from which the layer continues to growth during the deposition phase. This can be achieved by in situ process such as bias enhanced nucleation [29] in case of nanocrystalline diamond or by mechanical exfoliation and transfer to

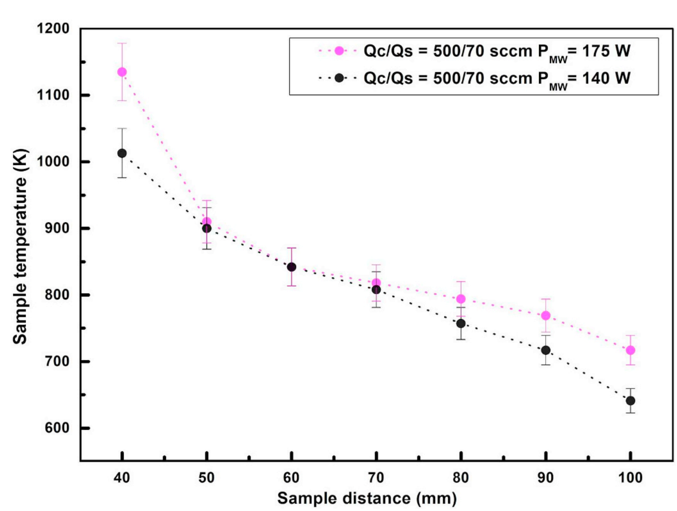

Fig. 3. Dependence of substrate temperature on delivered microwave power.

Table 1
Deposition conditions and Raman analysis of prepared samples.

Sample No	Qc (sccm)	Qs (sccm)	Qe (mg/min)	Pmw (W)	D (cm^{-1})	G (cm^{-1})	2D (cm^{-1})	2DFWHM (cm^{-1})	2D/G	D/G
GS35P175	500	35	2.2	175	NA	NA	NA	NA	NA	NA
GS70P175	500	70	4.5	175	1346	1585	2694	49	0.76	1.48
GS105P175	500	105	6.7	175	1345	1578	2692	42	1.59	1.02
GS140P175	500	140	8.9	175	1348	1581	2695	42	1.55	1.15
GS70P105	500	70	4.5	115	NA	NA	NA	NA	NA	NA
GS70P140	500	70	4.5	145	1347	1584	2685	56	2.05	1.29
GS70P140HT1	500	70	4.5	145	1345	1581	2689	63	0.94	3.48
GS70P140HT2	500	70	4.5	145	1344	1586	2695	79	0.39	2.59
GS70P140HT3	500	70	4.5	145	1348	1584	2696	60	1.01	1.07
GS300P420	360	300	19.2	420	1347	1579	2691	58	0.81	1.19
GS300P455	360	300	19.2	455	1346	1577	2691	59	1.29	1.1

substrate in the case of graphene [5]. In our experiment this process was represented by in situ formation of carbon nanostructures in microwave plasma in the vicinity of the substrate. At first, we investigated influence of precursor flow rate on the formation of graphene nanosheets and their deposition on the substrate. Because the aim of this study was to form single layer of graphene material on the substrate we chose low precursor liquid mass flow rates Qe from 2 to 9 mg/min of ethanol i.e. low flow rate of argon carrier gas Qs (35–140 sccm) through bubbler with liquid ethanol (Table 1). High flow rate of the ethanol Qs (500–1400 sccm) led to formation of large amount of deposit as shown in our previous work [26].

The substrate was placed 50 mm from the discharge nozzle. After the deposition whole substrate was covered with graphene nanosheets layer with small inhomogeneities around substrate edges due to the gas flow turbulence. Detailed SEM analysis of the substrates showed gradual increase of the density and size of graphene nanosheets on the surface as can be seen on Fig. 4.

For lowest flow rate only very small carbon nanoparticles could be found on the substrate. Median nanoparticle diameter of nanoparticles was 38 nm and nanoparticles covered 5% of the substrate surface. Further increase of ethanol flow rate led to graphene nanosheets coverage of the substrate and the coverage increased for flow rate of 70 sccm to 105 sccm, respectively. The area covered by the graphene nanosheets increased from 9 to 13% and median nanosheet size increased as well, from 83 to 146 nm, for higher flow rate. For flow rate of 140 sccm the amount of sheets substantially increased and they started to form 3D structure on the substrate. This result was in agreement with our observation of increase of C_2 molecules concentration with the increase of ethanol flow rate as determined by OES. C_2 molecule was main plasma species responsible for graphene nanosheets growth i.e. increase of their lateral size and amount. AFM analysis of substrate surface showed that the height of the nanosheets covering the substrate was between 1 and 2 nm. Raman analysis of samples showed presence of D (1345 cm^{-1}), G (1585 cm^{-1}) and 2D (2694 cm^{-1}) band in the

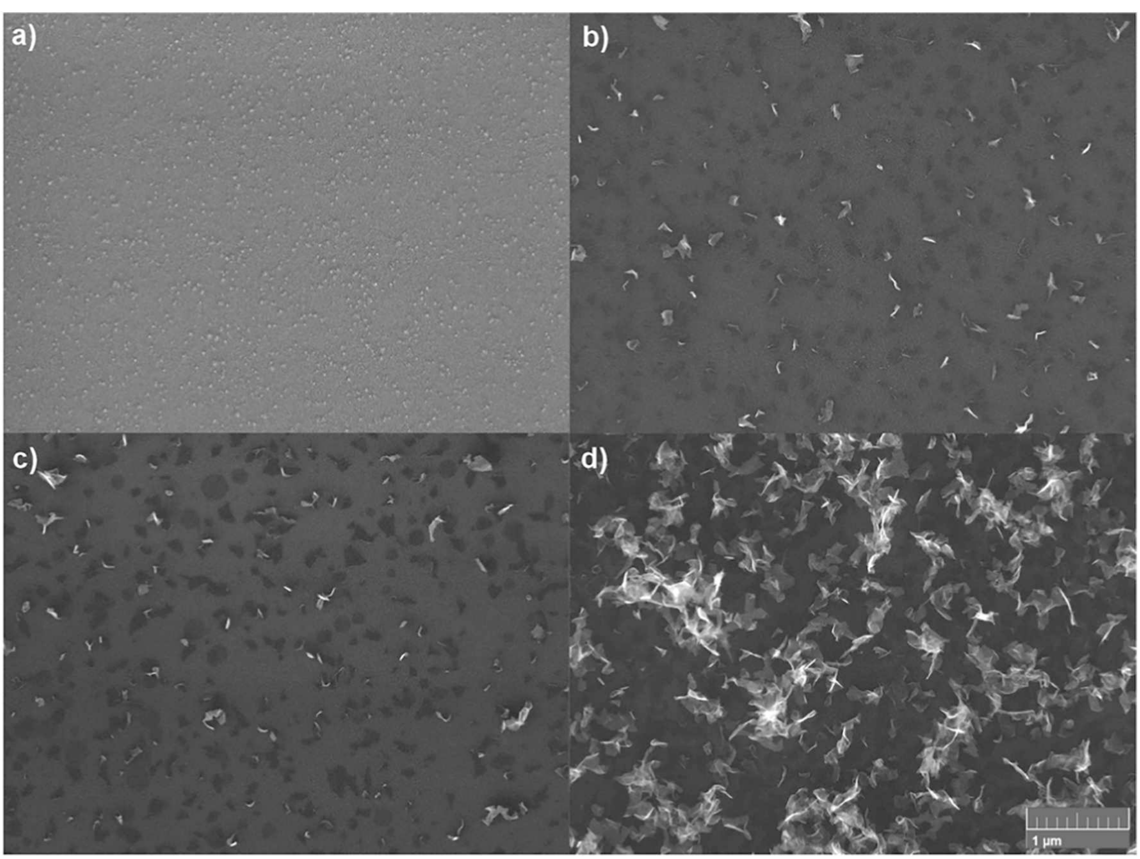

Fig. 4. SEM micrograph of deposited layers on Si/SiO_2 substrate for Qs a) 35 sccm b) 70 sccm c) 105 sccm and d) 140 sccm.

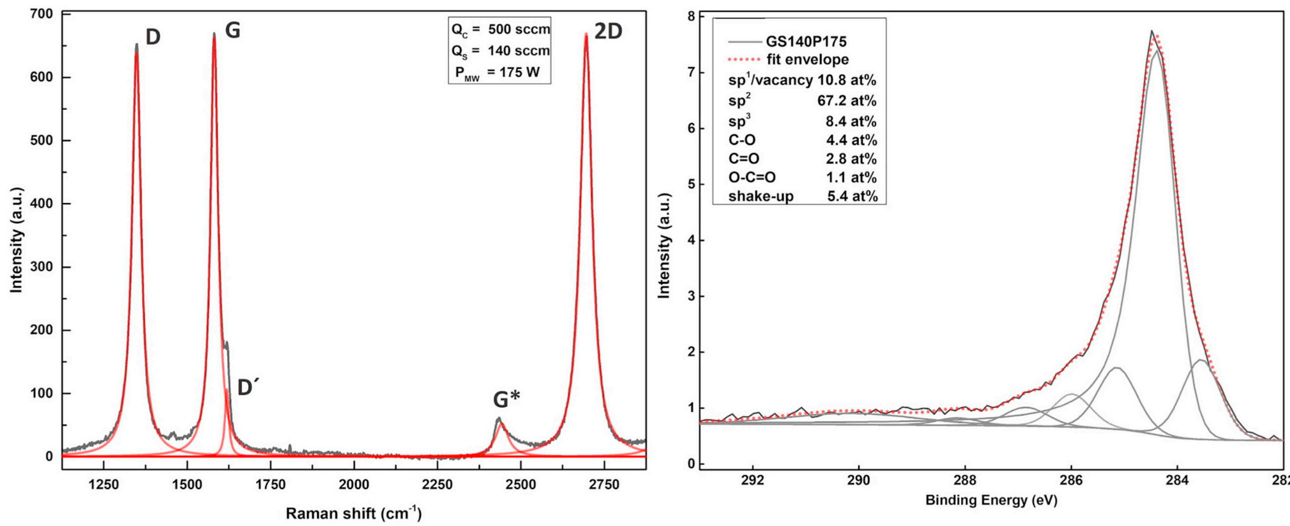

Fig. 5. Measured Raman spectra (black) with fitted peaks (red) of deposited layer for Qs of 140 sccm (left) and its XPS analysis (right). (For interpretation of the references to colour in this figure legend, the reader is referred to the web version of this article.)

Raman spectra (Fig. 5, left). For appropriate analysis of the Raman spectra, fitting of all bands with Lorentz peak was performed with exception of the D** band, where Gaussian profile is commonly used [30,31]. The peak positions, their full width at half maximum (FWHM) and intensity ratios can be found in Table 1. The reader should not misinterpret the zero intensity red line as background, since the Lorentz peaks were fitted without range restriction, thus it represent the gradual (quadratic) decline of Lorentz peak function to zero. The background was subtracted prior to peak fitting and was approximated by constant value in the whole measured range.

2D/G band intensity ratio increased from 0.8 to 1.6 with increase of Qs flow rate from 70 to 140 sccm, respectively. Only very weak signal with high noise was obtained on sample GS35P175 and the spectra could not be evaluated. The full width at half maximum (FWHM) of 2D band varied from 42 to 49 cm^{-1} corresponding to few layer graphene nanosheets [32] and was consistent with results of AFM, 0.34 nm per layer. Other bands observed in Raman spectra were D' at 1620 cm^{-1} corresponding to defects in the structure, and second order bands at 2450 cm^{-1} and 2940 cm^{-1} (D + G). As a consequence of very thin layer deposited on the substrate, silicon peak at 521 cm^{-1} and the second order modes between 900 and 1000 cm^{-1} were observed as well. XPS analysis and deconvolution of C1s peak region for sample with 140 sccm flow rate (Fig. 5, right) revealed presence of sp. (283.5 ± 0.1 eV), sp^2 (284.4 ± 0.1 eV), sp^3 (285.1 ± 0.1 eV) and oxygen related groups C—O (286.0 ± 0.2 eV), C═O (286.9 ± 0.2 eV) and O-C=O (288.1 ± 0.2 eV). Similarly, as in the case of well graphitised graphene nanosheets [26], the dominant carbon phase was sp^2 hybridisation. However, the sp^2 peak was also complemented with 8.4 at.% of sp^3 phase and also, a peak at lower binding energies, was observed which is mostly assigned to sp. hybridized carbon [33] or vacancies in the nanosheet structure [34,35]. TEM analysis of synthesized nanosheets (Fig. 6a) showed few-layer graphene structure with interlayer distance of 0.34 nm (image inset). The size and thickness of the nanosheets was consistent with results of SEM and curved and overlapping edges of the nanosheets could be observed as well. This can be seen in detail in the inset of Fig. 6a, were gradual increase of nanosheet thickness by two layers can be seen on top left forming few-layer graphene structure (FLG). FFT analysis of the in-plane structure in the bottom right section showed 6-fold symmetry of overlapping twisted bilayer (TBL) by 29° consistent with observations of Limbu et al. [36] and Wong et al. [37]. The formation of curved edges is known phenomena to minimize energy of nanosheet structure due to the presence of high energy dangling bonds on its edges [38]. The presence of the corrugations, edges and topological defects caused the relatively high intensity of D band in our samples in comparison with CVD growth graphene. The degree of disorder in our graphene nanosheets can be seen in Fig. 6b, were single layer structure (1 L), as proved by 6 single points in its FFT image analysis (Fig. 6b inset), is overlaid with incomplete second (2 L) and third layer (3 L). These observations are in agreement with TEM analysis of graphene nanosheets by Dato et al. [15]. We did not observe any carbon nanotubes in SEM or TEM micrographs.

3.3. Influence of delivered microwave power on deposition of graphene layer

We further investigated influence of delivered microwave power on carbon nanostructures deposited on the substrate. Delivered microwave power was limited by discharge stability. In regime with low precursor flow rate, below Qs of 100 sccm, the discharge became unstable for microwave power of 200 W and more. In this regime stable discharge transitioned into pulsing mode with high erosion of the electrode and contamination of the deposited layer. Low power mode was investigated for P_{MW} of 105 W and 145 W for Qs flow rate of 70 sccm. The samples were placed 50 mm from the carbon nozzle and the substrate temperature was 900 K. The result of deposition with low delivered microwave power can be seen Fig. 7.

Similarly to the deposition conditions of GS35P175 sample with P_{MW} of 175 W, we obtained small carbon nanostructures with median nanoparticle diameter of 48 nm but their density on the substrate was lower under selected conditions, area covered by the nanoparticles was 2%. For the intermediate setting of 145 W, we could observe sparse carbon nanosheets on the substrate. The area covered by the nanosheets was around 1.5% and their size was around 350 nm. Microwave power, 105 vs 175 W, had thus much higher influence on the deposition of carbon nanostructures and horizontally aligned graphene nanosheets than precursor flow rate (70 vs 35 sccm). This can be explained by different concentration of C_2 molecules in the discharge, due to lower decomposition rate of ethanol. The decomposition rate was influenced by plasma dynamics and its temperature that was 3100 and 3800 K for 105 and 145 W, respectively. Raman spectroscopy of sample GS70P140 (Fig. 8) showed high intensity of 2D band at 2685 cm^{-1} with FWHM of 56 cm^{-1} corresponding to bi- or trilayer graphene nanosheets.

High power mode was represented by delivered microwave power of 420 and 455 W. In this case the size of the plasma increased substantially and the substrate had to be placed 10 cm from the carbon

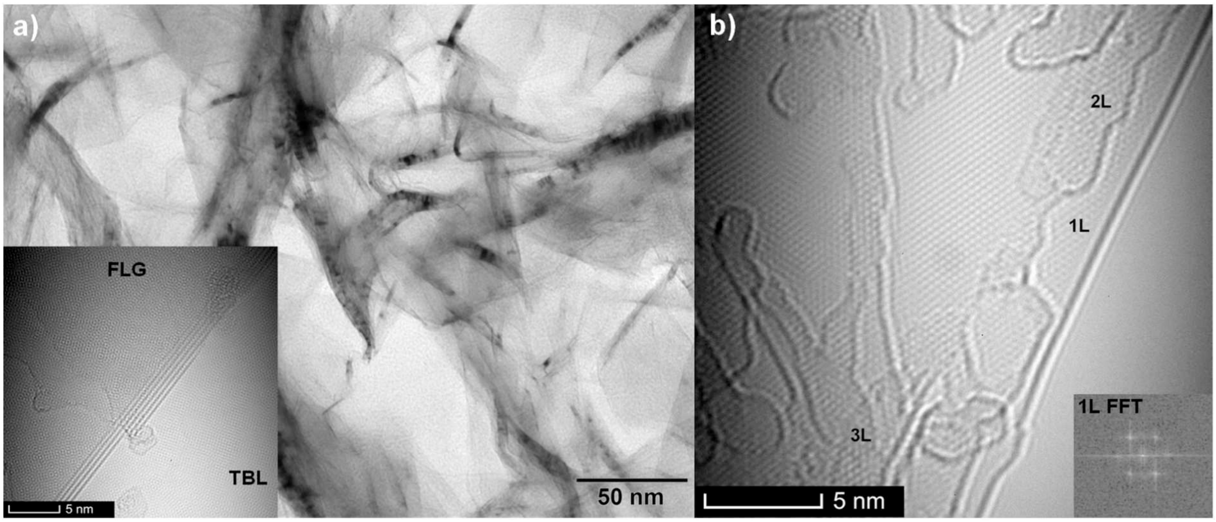

Fig. 6. TEM analysis a) of graphene nanosheets synthesized in microwave plasma torch (deposition time 5 min, substrate distance 300 mm) with detail of few-layer graphene layer and b) detail of single layer graphene nanosheet with overlaid second and third layer, inset- single layer FFT analysis.

nozzle. To obtain the stable plasma the central channel flow rate was lowered to 360 sccm and Qs flow rate was increased to 300 sccm. The deposition time was 300 s and the substrate temperature was 870 and 940 K for 420 and 455 W, respectively. SEM analysis of the sample showed mixture of carbon nanoparticles with embedded graphene nanosheets as can be seen in Fig. 9.

Raman spectroscopy of the sample showed broad structure of the D peak at 1347 cm^{-1} which was fitted with shoulder peaks D* and D** at 1250 and 1500 cm^{-1} (Fig. 10, left). The highly defective structure was caused by high content of carbon atoms and C_2 molecules in the plasma which resulted in growth of amorphous phase in the gas phase and which was deposited on the substrate and continued to grow there. This was in agreement with results of Dato et al. [15] where high content of free carbon atoms led to formation of amorphous phase. This result was further confirmed by XPS analysis of C1s spectra of the sample (Fig. 10, right). The content of sp^3 phase at 285.1 eV was 20.4 at.% and 44.5 at.% of sp^2 phase without a signal at lower binding energies signifying presence of sp. carbon phase as in previous, lower ethanol flow rate and microwave power case. Such high content of sp^3 phase together with an intensive D band region in Raman spectroscopy (especially the broad D** band) corresponded to the amorphous carbon nanoparticles structure. The content of carbon-oxygen bonds also increased to 29.1 at.%.

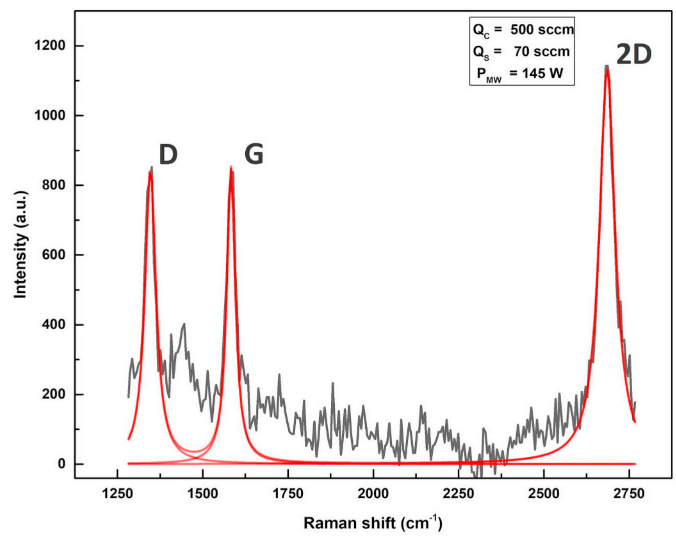

Fig. 8. Measured Raman spectrum (black) with peaks fitted (red) of graphene layer deposited at Qs 70 sccm and P_{MW} of 145 W. (For interpretation of the references to colour in this figure legend, the reader is referred to the web version of this article.)

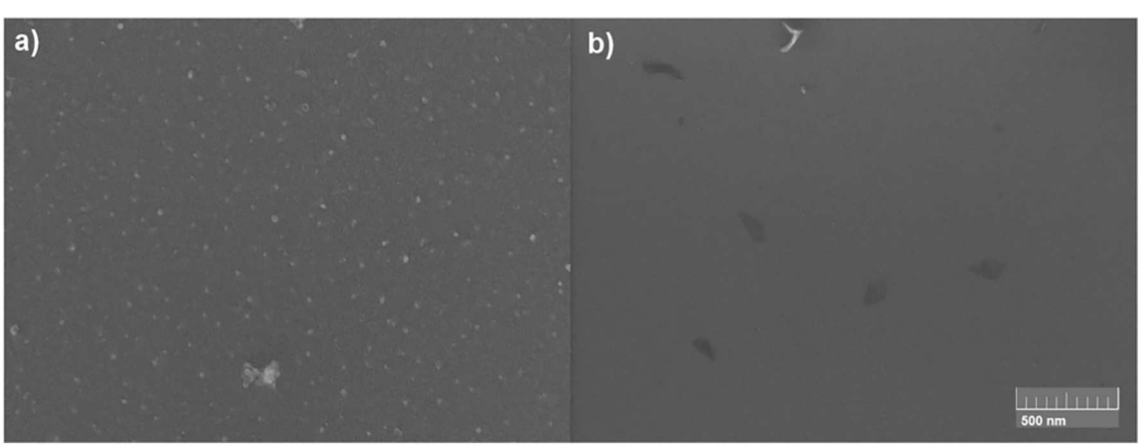

Fig. 7. SEM micrograph of graphene layers deposited at low power mode of a) 105 W and b) 145 W, substrate temperature 900 K.

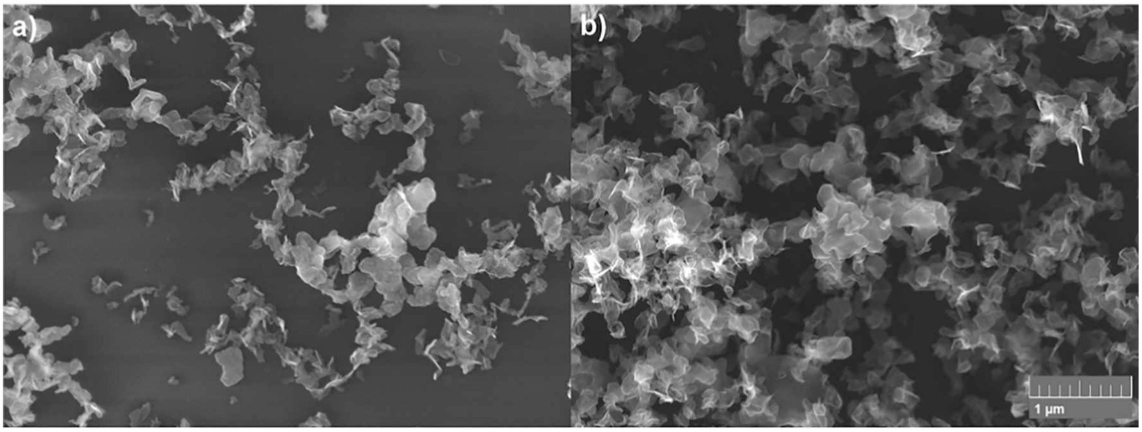

Fig. 9. Carbon layer deposited in high power mode Qc 360 sccm, Qs 300 sccm a) 420 W and b) 455 W.

3.4. Influence of close proximity of the plasma active zone on deposition of graphene layer

As discussed above, flow of growth species towards substrate surface played important role in the deposition process. Therefore we investigated the influence of close vicinity of the plasma region on the deposition process. In the experiment we used precursor flow rate of 70 sccm and applied microwave power of 140 W. The distance between the substrate and plasma nozzle was decreased to 40 mm. We also carried out this experiment also for P_{MW} of 175 W but at distance of 40 mm the silicon substrate was damaged at the point of contact with the plasma. Due to the very small distance between active plasma region, below 10 mm, there was an inhomogeneous flow of the active plasma species towards substrate surface and radial temperature profile was formed as well i.e. temperature in the center of the substrate was higher than at its edges. According to our measurement the substrate temperature was above 1000 K and as previously mentioned, at higher power, the silicon substrate could reach on the surface closest to the plasma melting temperature of silicon (1687 K). The results of the deposition can be seen in Fig. 11.

The analysis showed that the growth transitioned from horizontal to vertical with increasing flux of active plasma species and the substrate temperature. This observation was in agreement with work of Malesevic et al. [8] who suggested that the initial horizontal growth converts into vertical growth by partial cracking and delamination of nucleation layer. This conclusion was also supported by our early observation of layers deposited with variable flow rate, where part of the nanosheets edges was delaminated from the surface and formed natural nucleation sites for vertical growth. High temperature and high flux of C_2 were also suggested as necessary condition for the preferential growth of carbon nanowalls by Cheng et al. [39] during the synthesis of nanodiamond layers. Observed growth at the substrate temperature of 1000 K was also in agreement with the values between 970 and 1100 K reported by Bo et al. [10] and Meško et al. [12] for atmospheric pressure DC PECVD growth of carbon nanowalls. Raman spectra (Fig. 11, top right) of the graphene nanosheets in Fig. 11a exhibited high intensity D peak at 1345 cm^{-1} and D′ peak at 1608 cm^{-1} with low intensity of second order peaks. This observation was consistent with features found in Raman spectra of vertically aligned graphene.

4. Conclusions

Horizontally aligned layer of graphene nanosheets was successfully deposited on Si/SiO_2 substrate by decomposition of ethanol in dual-channel microwave plasma torch at atmospheric pressure. Median size and density of the graphene nanosheets forming the layer increased, from 83 to 146 nm, with increasing ethanol flow rate and delivered microwave power which determined amount of C atoms and C_2 molecules in the plasma. Simultaneously, the 2D/G band ratio increased from 0.76 to 1.55 and 2D peak FWHM decreased from 49 to 42 cm^{-1}. The composition of the carbon layer on the substrate could be changed

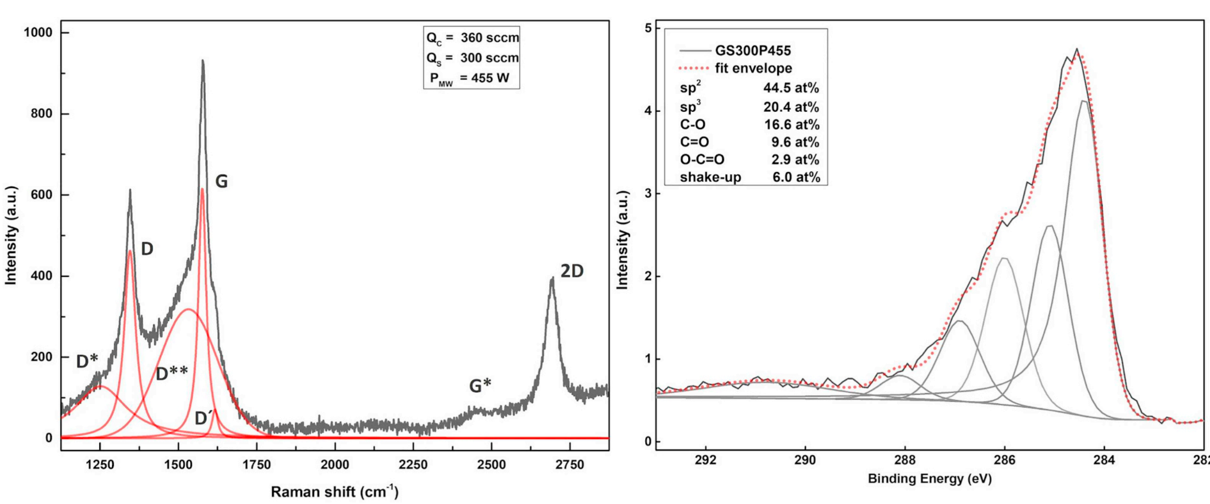

Fig. 10. Measured Raman spectra (black) with fitted peaks (red) of deposited layer for P_{MW} of 455 W (left) and its XPS analysis (right). (For interpretation of the references to colour in this figure legend, the reader is referred to the web version of this article.)

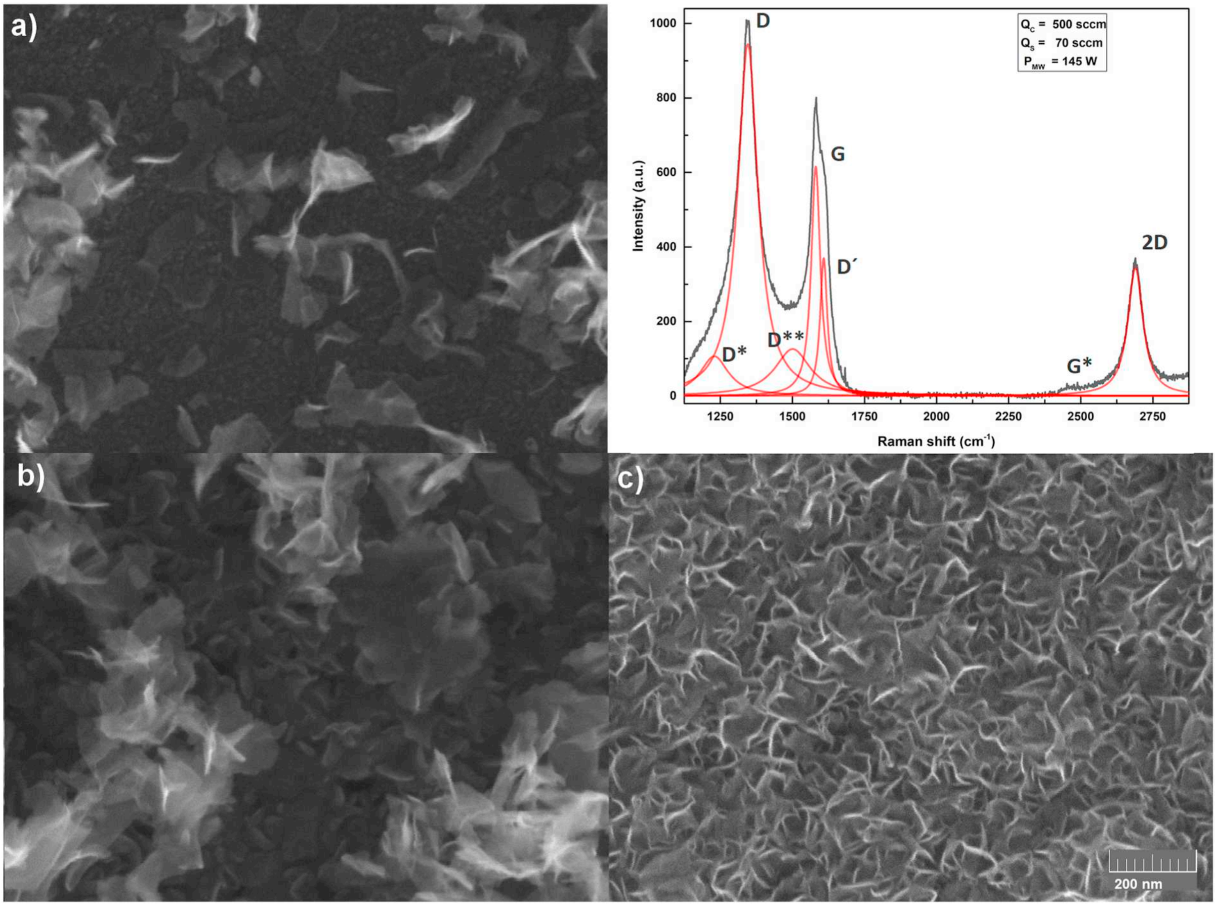

Fig. 11. Deposition of vertically oriented graphene with substrate in the vicinity of the discharge a) 3 mm from the edge of the substrate and its Raman spectra - measured spectra (black) and fitted peaks (red), b) 4 mm from the edge of the substrate and c) center of the substrate. (For interpretation of the references to colour in this figure legend, the reader is referred to the web version of this article.)

in controlled manner from horizontally aligned graphene nanosheets to vertically aligned few layer graphene by increasing substrate temperature above 1000 K or to amorphous carbon nanoparticles by increasing ethanol flow rate and delivered microwave power. For both types of layers, the intensity of D*, D and D** bands in Raman spectra increased substantially, with D/G band ratio between 1.2 and 3.5, while 2D/G band ratio decreased below 1. The amount of disorder in the amorphous nanoparticles structure was also accompanied with high content of 20.4 at.%. of sp^3 phase determined by deconvolution of C1s peak region in XPS spectra. The ability to controllably grow wide range of carbon based layers directly on dielectric substrate using simple precursor at atmospheric pressure plasma system represents unique opportunity for future applications such as transparent conductive layers, sensors and carbon functional coatings.

CRediT authorship contribution statement

Ondřej Jašek:Conceptualization, Investigation, Writing - original draft, Writing - review & editing.**Jozef Toman**:Investigation, Formal analysis, Writing - original draft.**Jana Jurmanová**: Investigation.**Miroslav Šnírer**:Investigation, Writing - original draft.**Vít Kudrle**:Writing - review & editing.**Vilma Buršíková**:Investigation.

Declaration of competing interest

The authors declare that they have no known competing financial interests or personal relationships that could have appeared to influence the work reported in this paper.

Acknowledgements

This work was supported by the Czech Science Foundation under project 18-08520S and in part by project LM2018097 funded by The Ministry of Education, Youth and Sports of the Czech Republic. We acknowledge CEITEC Nano Research Infrastructure supported by MEYS CR (LM2018110). We would like to thank Jiri Bursik for TEM analysis.

References

[1] A.C. Ferrari, F. Bonaccorso, V. Fal'ko, K.S. Novoselov, S. Roche, P. Bøggild, S. Borini, F.H.L. Koppens, V. Palermo, N. Pugno, J.A. Garrido, R. Sordan, A. Bianco, L. Ballerini, M. Prato, E. Lidorikis, J. Kivioja, C. Marinelli, T. Ryhänen, A. Morpurgo, J.N. Coleman, V. Nicolosi, L. Colombo, A. Fert, M. Garcia-Hernandez, A. Bachtold, G.F. Schneider, F. Guinea, C. Dekker, M. Barbone, Z. Sun, C. Galiotis, A.N. Grigorenko, G. Konstantatos, A. Kis, M. Katsnelson, L. Vandersypen, A. Loiseau, V. Morandi, D. Neumaier, E. Treossi, V. Pellegrini, M. Polini, A. Tredicucci, G.M. Williams, B.H. Hong, J.-H. Ahn, J.M. Kim, H. Zirath, B.J. van Wees, H. van der Zant, L. Occhipinti, A. Di Matteo, I.A. Kinloch, T. Seyller, E. Quesnel, X. Feng, K. Teo, N. Rupesinghe, P. Hakonen, S.R.T. Neil, Q. Tannock, T. Löfwander, J. Kinaret, Science and technology roadmap for graphene, related two-dimensional crystals, and hybrid systems, Nanoscale 7 (2015) 4598–4810.

[2] F. Bonaccorso, A. Lombardo, T. Hasan, Z. Sun, L. Colombo, A.C. Ferrari, Production and processing of graphene and 2d crystals, Mater. Today 15 (2012) 564–589, https://doi.org/10.1016/s1369-7021(13)70014-2.

[3] A. Dato, Graphene synthesized in atmospheric plasmas—a review, J. Mater. Res. 34 (2019) 214–230, https://doi.org/10.1557/jmr.2018.470.

[4] Q.-Q. Zhuo, Q. Wang, Y.-P. Zhang, D. Zhang, Q.-L. Li, C.-H. Gao, Y.-Q. Sun, L. Ding, Q.-J. Sun, S.-D. Wang, J. Zhong, X.-H. Sun, S.-T. Lee, Transfer-free synthesis of doped and patterned graphene films, ACS Nano 9 (2015) 594–601.

[5] D. Wei, Y. Lu, C. Han, T. Niu, W. Chen, A.T.S. Wee, Critical crystal growth of graphene on dielectric substrates at low temperature for electronic devices, Angew. Chem. Int. Ed. Eng. 52 (2013) 14121–14126.

[6] D. Wei, L. Peng, M. Li, H. Mao, T. Niu, C. Han, W. Chen, A.T.S. Wee, Low

temperature critical growth of high quality nitrogen doped graphene on dielectrics by plasma-enhanced chemical vapor deposition, ACS Nano 9 (2015) 164–171.
[7] M. Meyyappan, J.-S. Lee, Graphene growth by plasma-enhanced chemical vapor deposition (PECVD), Plasma Processing of Nanomaterials (2017) 231–243, https://doi.org/10.1201/b11473-9.
[8] A. Malesevic, R. Vitchev, K. Schouteden, A. Volodin, L. Zhang, G. Van Tendeloo, A. Vanhulsel, C. Van Haesendonck, Synthesis of few-layer graphene via microwave plasma-enhanced chemical vapour deposition, Nanotechnology 19 (2008) 305604.
[9] Z. Bo, Y. Yang, J. Chen, K. Yu, J. Yan, K. Cen, Plasma-enhanced chemical vapor deposition synthesis of vertically oriented graphene nanosheets, Nanoscale 5 (2013) 5180–5204.
[10] Z. Bo, K. Yu, G. Lu, P. Wang, S. Mao, J. Chen, Understanding growth of carbon nanowalls at atmospheric pressure using normal glow discharge plasma-enhanced chemical vapor deposition, Carbon 49 (2011) 1849–1858, https://doi.org/10.1016/j.carbon.2011.01.007.
[11] K. Yu, Z. Bo, G. Lu, S. Mao, S. Cui, Y. Zhu, X. Chen, R.S. Ruoff, J. Chen, Growth of carbon nanowalls at atmospheric pressure for one-step gas sensor fabrication, Nanoscale Res. Lett. 6 (2011) 202.
[12] M. Meško, V. Vretenár, P. Kotrusz, M. Hulman, J. Šoltýs, V. Skákalová, Carbon nanowalls synthesis by means of atmospheric dcPECVD method, Phys. Status Solidi B 249 (2012) 2625–2628, https://doi.org/10.1002/pssb.201200144.
[13] A. Vesel, R. Zaplotnik, G. Primc, M. Mozetič, Synthesis of vertically oriented graphene sheets or carbon nanowalls-review and challenges, Materials. 12 (2019). doi:https://doi.org/10.3390/ma12182968.
[14] N.M. Santhosh, G. Filipič, E. Tatarova, O. Baranov, H. Kondo, M. Sekine, M. Hori, K. K. Ostrikov, U. Cvelbar, Oriented carbon nanostructures by plasma processing: recent advances and future challenges, Micromachines (Basel). 9 (2018). doi:https://doi.org/10.3390/mi9110565.
[15] A. Dato, M. Frenklach, Substrate-free microwave synthesis of graphene: experimental conditions and hydrocarbon precursors, New J. Phys. 12 (2010) 125013, https://doi.org/10.1088/1367-2630/12/12/125013.
[16] E. Tatarova, A. Dias, J. Henriques, A.M.B. do Rego, A.M. Ferraria, M.V. Abrashev, C. C. Luhrs, J. Phillips, F.M. Dias, C.M. Ferreira, Microwave plasmas applied for the synthesis of free standing graphene sheets, Journal of Physics D: Applied Physics. 47 (2014) 385501. doi:https://doi.org/10.1088/0022-3727/47/38/385501.
[17] D. Tsyganov, N. Bundaleska, E. Tatarova, A. Dias, J. Henriques, A. Rego, A. Ferraria, M.V. Abrashev, F.M. Dias, C.C. Luhrs, J. Phillips, On the plasma-based growth of "flowing" graphene sheets at atmospheric pressure conditions, Plasma Sources Sci. Technol. 25 (2016) 015013, , https://doi.org/10.1088/0963-0252/25/1/015013.
[18] C. Melero, R. Rincón, J. Muñoz, G. Zhang, S. Sun, A. Perez, O. Royuela, C. González-Gago, M.D. Calzada, Scalable graphene production from ethanol decomposition by microwave argon plasma torch, Plasma Phys. Controlled Fusion 60 (2018) 014009, , https://doi.org/10.1088/1361-6587/aa8480.
[19] R. Rincón, C. Melero, M. Jiménez, M.D. Calzada, Synthesis of multi-layer graphene and multi-wall carbon nanotubes from direct decomposition of ethanol by microwave plasma without using metal catalysts, Plasma Sources Sci. Technol. 24 (2015) 032005, , https://doi.org/10.1088/0963-0252/24/3/032005.
[20] R. Rincón, M. Jiménez, J. Muñoz, M. Sáez, M.D. Calzada, Hydrogen production from ethanol decomposition by two microwave atmospheric pressure plasma sources: surfatron and TIAGO torch, Plasma Chem. Plasma Process. 34 (2014) 145–157, https://doi.org/10.1007/s11090-013-9502-4.
[21] N. Bundaleska, N. Bundaleski, A. Dias, F.M. Dias, M. Abrashev, G. Filipič, U. Cvelbar, Z. Rakočević, Z. Kissovski, J. Henriques, E. Tatarova, Microwave N2-Ar plasmas applied for N-graphene post synthesis, Mater. Res. Express 5 (2018) 095605, , https://doi.org/10.1088/2053-1591/aad7e9.
[22] N. Bundaleska, J. Henriques, M. Abrashev, A.M. Botelho do Rego, A.M. Ferraria, A. Almeida, F.M. Dias, E. Valcheva, B. Arnaudov, K.K. Upadhyay, M.F. Montemor, E. Tatarova, Large-scale synthesis of free-standing N-doped graphene using microwave plasma, Sci. Rep. 8 (2018) 12595.
[23] O. Jašek, M. Eliáš, L. Zajíčková, Z. Kučerová, J. Matějková, A. Rek, J. Buršík, Discussion of important factors in deposition of carbon nanotubes by atmospheric pressure microwave plasma torch, J. Phys. Chem. Solids 68 (2007) 738–743, https://doi.org/10.1016/j.jpcs.2007.01.039.
[24] A.G. Bannov, O. Jasek, A. Manakhov, M. Marik, D. Necas, L. Zajickova, High-performance ammonia gas sensors based on plasma treated carbon nanostructures, IEEE Sensors J. 17 (2017) 1964–1970, https://doi.org/10.1109/jsen.2017.2656122.
[25] A.G. Bannov, J. Prášek, O. Jašek, L. Zajíčková, Investigation of pristine graphite oxide as room-temperature chemiresistive ammonia gas sensing material, Sensors. 17 (2017). doi:https://doi.org/10.3390/s17020320.
[26] J. Toman, O. Jasek, M. Snirer, V. Kudrle, J. Jurmanova, On the interplay between plasma discharge instability and formation of free-standing graphene nanosheets in a dual-channel microwave plasma torch at atmospheric pressure, J. Phys. D. Appl. Phys. 52 (2019) 265205, https://doi.org/10.1088/1361-6463/ab0f69.
[27] J. Voráč, P. Synek, L. Potočňáková, J. Hnilica, V. Kudrle, Batch processing of overlapping molecular spectra as a tool for spatio-temporal diagnostics of power modulated microwave plasma jet, Plasma Sources Sci. Technol. 26 (2017) 025010, , https://doi.org/10.1088/1361-6595/aa51f0.
[28] R. Rincón, J. Muñoz, M. Sáez, M.D. Calzada, Spectroscopic characterization of atmospheric pressure argon plasmas sustained with the Torche à Injection Axiale sur Guide d'Ondes, Spectrochim. Acta B At. Spectrosc. 81 (2013) 26–35, https://doi.org/10.1016/j.sab.2012.12.006.
[29] W. Kulisch, L. Ackermann, B. Sobisch, On the mechanisms of bias enhanced nucleation of diamond, Phys. Status Solidi A 154 (1996) 155–174, https://doi.org/10.1002/pssa.2211540113.
[30] T. Jawhari, A. Roid, J. Casado, Raman spectroscopic characterization of some commercially available carbon black materials, Carbon 33 (1995) 1561–1565, https://doi.org/10.1016/0008-6223(95)00117-v.
[31] A. Sadezky, H. Muckenhuber, H. Grothe, R. Niessner, U. Pöschl, Raman microspectroscopy of soot and related carbonaceous materials: spectral analysis and structural information, Carbon. 43 (2005) 1731–1742, https://doi.org/10.1016/j.carbon.2005.02.018.
[32] A.C. Ferrari, J.C. Meyer, V. Scardaci, C. Casiraghi, M. Lazzeri, F. Mauri, S. Piscanec, D. Jiang, K.S. Novoselov, S. Roth, A.K. Geim, Raman spectrum of graphene and graphene layers, Phys. Rev. Lett. 97 (2006) 187401.
[33] M. Rybachuk, J.M. Bell, Electronic states of trans-polyacetylene, poly(p-phenylene vinylene) and sp-hybridised carbon species in amorphous hydrogenated carbon probed by resonant Raman scattering, Carbon 47 (2009) 2481–2490, https://doi.org/10.1016/j.carbon.2009.04.049.
[34] A. Barinov, O. Bariş Malcioğlu, S. Fabris, T. Sun, L. Gregoratti, M. Dalmiglio, M. Kiskinova, Initial stages of oxidation on graphitic surfaces: photoemission study and density functional theory calculations, J. Phys. Chem. C 113 (2009) 9009–9013, https://doi.org/10.1021/jp902051d.
[35] K. Ganesan, S. Ghosh, N.G. Krishna, S. Ilango, M. Kamruddin, A.K. Tyagi, A comparative study on defect estimation using XPS and Raman spectroscopy in few layer nanographitic structures, Phys. Chem. Chem. Phys. 18 (2016) 22160–22167, https://doi.org/10.1039/c6cp02033j.
[36] T.B. Limbu, J.C. Hernández, F. Mendoza, R.K. Katiyar, J.J. Razink, V.I. Makarov, B.R. Weiner, G. Morell, A novel approach to the layer-number-controlled and grain-size-controlled growth of high quality graphene for nanoelectronics, ACS Appl. Nano Mater. 1 (2018) 1502–1512, https://doi.org/10.1021/acsanm.7b00410.
[37] H.S. Wong, C. Durkan, Unraveling the rotational disorder of graphene layers in graphite, Physical Review B. 81 (2010). doi:https://doi.org/10.1103/physrevb.81.045403.
[38] G. Yang, L. Li, W.B. Lee, M.C. Ng, Structure of graphene and its disorders: a review, Sci. Technol. Adv. Mater. 19 (2018) 613–648.
[39] C.Y. Cheng, K. Teii, Control of the growth regimes of nanodiamond and nanographite in microwave plasmas, IEEE Trans. Plasma Sci. 40 (2012) 1783–1788, https://doi.org/10.1109/tps.2012.2198487.